Plasma Sources Science and Technology

PAPER

Theoretical study of dissociative recombination and vibrational excitation of the BF_2^+ ion by an electron impact

To cite this article: Viatcheslav Kokoouline *et al* 2018 *Plasma Sources Sci. Technol.* **27** 115007

IOP Publishing Plasma Sources Science and Technology
Plasma Sources Sci. Technol. **27** (2018) 115007 (6pp) https://doi.org/10.1088/1361-6595/aae6f7

Theoretical study of dissociative recombination and vibrational excitation of the BF_2^+ ion by an electron impact

Viatcheslav Kokoouline[1,7], Mehdi Ayouz[2], János Zsolt Mezei[3,4,5,7], Khalid Hassouni[4] and Ioan F Schneider[5,6]

[1] Department of Physics, University of Central Florida, Orlando, FL 32816, United States of America
[2] LGPM, CentraleSupelec, Université Paris-Saclay, 8-10 Rue Joliot Curie, F-91190 Gif-sur-Yvette, France
[3] Institute for Nuclear Research, Hungarian Academy of Sciences, H-4001 Debrecen, Hungary
[4] Laboratoire des Sciences des Procédés et des Matériaux, CNRS-UPR3407, Université Paris 13, F-93430 Villetaneuse, France
[5] Laboratoire Ondes et Milieux Complexes CNRS-UMR6294, Université du Havre, F-76058 Le Havre, France
[6] Laboratoire Aimé Cotton CNRS-UMR9188, Université Paris-Sud, ENS Cachan, Université Paris-Saclay, F-91405 Orsay, France

E-mail: Viatcheslav.Kokoouline@ucf.edu and mezei.zsolt@atomki.mta.hu

Received 9 July 2018, revised 17 September 2018
Accepted for publication 9 October 2018
Published 7 November 2018

Abstract

Cross-sections for dissociative recombination and electron-impact vibrational excitation of the BF_2^+ molecular ion are computed using a theoretical approach that combines the normal modes approximation for the vibrational states of the target ion and use of the UK R-matrix code to evaluate electron–ion scattering matrices for fixed geometries of the ion. Thermally-averaged rate coefficients are obtained from the cross-sections for temperatures in the 10–3000 K range.

Keywords: non-equilibrium plasmas, plasma immersion ion implantation, electron molecular cation reactive collisions, dissociative recombination, vibrational excitation, vibrational frame transformation, R-matrix theory

1. Introduction

Non-equilibrium plasmas produced by electrical discharges in BF_3-containing feed gas are of continually increasing interest for a large number of applications. In particular, BF_3 is very often the boron carrier when plasmas are used for material processing [1–3]. Basically, BF_3 plasmas are used either for (i) the synthesis of ultra-hard boron compounds, e.g. boron carbides [1], (ii) the deposition of boron nitride, an advanced material with a large number of functionalities [2], and (iii) p-type doping by boron in the semi-conductor and photo-voltaic industries [3, 4]. As far as doping applications are concerned, plasma immersion ion implantation (PIII) processes are probably one of the most promising in terms of cost and technical performance [4, 5]. These processes make use of very low pressure, very high density magnetized plasmas generated in a BF_3-containing feed gas. Depending on the level of the power coupled to the plasma, several cations—BF_3^+, BF_2^+, BF^+, B^+—and anions—e.g. F^-—may be produced [6, 7]. The positive ions are then extracted from the source to an implantation chamber where the processed silicon substrate is submitted to very high negative voltage pulses. These pulses result in a large acceleration of the positive ions that are implanted in the substrate, which results in the doping of the latter. The implantation depth depends on the nature and the energy distribution of the ions impinging the substrate, while the doping level depends on the ion flux and, consequently, on the plasma density. The plasma density and the relative predominance of the different ions are determined by the ionization kinetics in the source region. The plasma sources used in PIII processes are usually magnetized [8]. The ambipolar diffusion in the radial direction

[7] Authors to whom any correspondence should be addressed.

that is perpendicular to the magnetic field is strongly reduced with respect to the parallel diffusion. Under typical plasma conditions used in PIII processes, i.e., $B \approx 100-500$ G and $p \approx 1$ Pa, electron cyclotron frequency in the GHz range, while the electron-neutral momentum transfer collision frequency is in the MHz range, according to equation (5.4.5) of [9] the diffusion coefficient in the radial direction is reduced by approximately 6 orders of magnitude with respect to the parallel diffusion coefficient. The characteristic time estimated for perpendicular diffusion for typical PIII reactor geometries is at the order of 100 s, while the dissociative recombination (DR) characteristic time is around 0.1 s. Following a similar procedure, one can easily show that mutual neutralization is also likely to dominate diffusion losses provided the negative ion density is of the same order of magnitude as the electron density, i.e. moderately electronegative plasmas. It appears, therefore, that under PIII discharge conditions, positive ion losses at the reactor wall are dominated by their DR with electrons and by their neutralization through collisions with negative ions. The investigation of DR of molecular ions is therefore of major interest for these processes. This is especially the case with BF_2^+, which is often the major ion in BF_3-containing plasma in discharge conditions corresponding to PIII process [5]. This study is a continuation of a previous work performed in the theoretical framework of the multichannel quantum defect theory on the DR and competitive processes of BF^+ [10].

The article is organized as follows. After the Introduction, section 2 describes the theoretical approach used in the present calculation. In section 3, the obtained cross-sections and the corresponding rate coefficients are displayed and discussed. Section 4 concludes the study.

2. Theoretical approach

2.1. Dissociative recombination and vibrational excitation cross-section formulas

Since the basic formalism used in our model is presented in detail in [11, 12], we restrict ourselves here to underlining its major ideas. The molecular cation under study, BF_2^+, is linear in its equilibrium geometry.

The theoretical model starts with the following assumptions (see for example [12]): (i) the rotation of the molecule is neglected, (ii) the cross-section is averaged over the autoionizing resonances, (iii) the autoionization lifetime is assumed to be much longer than the predissociation lifetime and (iv) the harmonic approximation is used to describe the vibrational state of the core ion. Using (i)–(iv) and applying the frame transformation, the DR cross-section is given by equation (13) of [12], in which the scattering matrix elements were expanded to first order in the normal coordinates. The cross-section for vibrational excitation (VE) of the mode i is written as

$$\sigma_i^{\mathrm{VE}}(E_{\mathrm{el}}) = \frac{\pi\hbar^2}{4\,mE_{\mathrm{el}}} g_i \sum_{ll'\lambda\lambda'} \left| \frac{\partial S_{l\lambda,l'\lambda'}}{\partial q_i} \right|^2 \theta(E_{\mathrm{el}} - \hbar\omega_i). \quad (1)$$

Here q_i, $\hbar\omega_i$ and g_i ($i = 1, 2, 3$) are respectively the dimensionless coordinate, the energy and the degeneracy of the mode i. The degeneracy is two for the bending mode 2 and one for the symmetric and asymmetric stretching modes. $S_{l\lambda,l'\lambda'}$ is an element of the fixed-nuclei scattering matrix for electron–BF_2^+ collisions with initial channel (λl) and exit channel ($\lambda' l'$), l being the electron angular momentum and λ its projection on the molecular axis. Finally, m is the reduced mass of the electron–ion system, E_{el} the incident energy of the electron and θ the Heaviside step function. The present theoretical approach can describe the (de-)excitation process changing only one quantum in each normal mode of the target ion. (De-)excitation cross-sections for changing two or more quanta in a mode are much smaller (the propensity rule) and are neglected in this study. In the present case, the initial state of the ion is the ground vibrational level, so the electron can only be captured into the first excited vibrational state of each normal mode.

The situation is similar if the electron energy is not sufficient to excite the ion and then to leave it. In such a situation, the present model suggests that the probability of excitation of the ion by the electron is described by the same physics, but instead of leaving the vibrationally excited ion, the electron is captured in a Rydberg resonance attached to that vibrational state, excited by the electron. If the electron is captured by the ion, the system will most likely dissociate, rather then autoionize. Correspondingly, the cross-section for DR is then obtained [12] as

$$\sigma^{\mathrm{DR}}(E_{\mathrm{el}}) = \frac{\pi\hbar^2}{4\,mE_{\mathrm{el}}} \sum_{i=1}^{3} g_i \sum_{ll'\lambda\lambda'} \left| \frac{\partial S_{l\lambda,l'\lambda'}}{\partial q_i} \right|^2 \theta(\hbar\omega_i - E_{\mathrm{el}}). \quad (2)$$

Here i runs over all three modes: two stretching modes ν_1 and ν_3 (symmetric and asymmetric) with respective frequencies ω_1 and ω_3 and corresponding coordinates q_1 and q_3, and a doubly degenerate transverse mode ν_2 with a lower frequency ω_2 and coordinates (q_{2x}, q_{2y}).

To calculate the derivative of the scattering matrix $\partial S_{l\lambda,l'\lambda'}/\partial q_i$ with respect to the normal coordinate q_i, the scattering matrix is evaluated for two values of q_i keeping the other normal coordinates $q_{i'}$ fixed at $q_{i'} = 0$.

The elements $S_{l\lambda,l'\lambda'}(\vec{q})$ of the scattering matrix $\hat{S}(\vec{q})$ at a given geometry $\vec{q}$ specified by four normal coordinates $\vec{q} = \{q_1, q_2, q_3, q_4\} = \{q_1, q_{2x}, q_3, q_{2y}\}$ are computed from the reactance matrix $\hat{K}$, obtained numerically as discussed below:

$$\hat{S} = \frac{\hat{1} + i\hat{K}}{\hat{1} - i\hat{K}}, \quad (3)$$

where $\hat{1}$ is the identity matrix.

2.2. The properties of the BF_2^+ ion and the scattering calculations

The main electronic ground state configuration $^1\Sigma_g^+$ of the ion in its natural point group symmetry $D_{\infty h}$ is $(1\sigma_u^+)^2$ $(1\sigma_g^+)^2$ $(2\sigma_g^+)^2$ $(2\sigma_u^+)^2$ $(3\sigma_g^+)^2$ $(4\sigma_g^+)^2$ $(3\sigma_u^+)^2$ $(1\pi_u^-)^2$ $(1\pi_u^+)^2$ $(1\pi_g^-)^2$ $(1\pi_g^+)^2$. The normal coordinates and the related frequencies are obtained using the cc-pVTZ basis set centered on each atom

Table 1. Vibrational frequencies (in cm^{-1}) obtained in this study and compared with previous data available in literature.

Mode	Symmetric stretching	Bending	Asymmetric stretching		
Symmetry	Σ_g^+	Π_u^+ and Π_u^-	Σ_u^+		
	ω_1	ω_2	ω_3	Method	References
	1062.8	469.2	2146.1	CI/cc-pVTZ	This work
	1023	443	2088	MP2	[14]
	1030	450		CI	[15]
			2 026.1 ± 0.2	Exp.	[16]

and including *s*, *p* and *d* orbitals. Performing configuration interaction (CI) calculations in the D_{2h} symmetry group, using the MOLPRO suite of codes [13], we found that the equilibrium geometry of the ion has a B–F distance of 1.2215 Å. Table 1 gives the vibrational frequencies obtained from CI calculations using the cc-pVTZ basis set, and compares with the data available in literature.

The electron-scattering calculations were performed using the UK R-Matrix code [17, 18] with the Quantemol-N interface [19]. The calculations were performed in the abelian subgroup D_{2h} and the target BF_2^+ ion was assumed to be in its ground electronic state. In our CI model, we freeze 10 electrons in the core $1a_g$, $2a_g$, $3a_g$, $1b_{2u}$, $2b_{2u}$, while the remaining 12 electrons are kept free in the active space of the $4a_g$, $5a_g$, $1b_{3u}$, $2b_{3u}$, $3b_{2u}$, $4b_{2u}$, $1b_{1g}$, $1b_{1u}$, $2b_{1u}$, $1b_{3g}$ molecular orbitals. A total of eight electronic excited target states are represented by 1844 configuration state functions (CSFs) for the ground state. All the generated states up to 16 eV were retained in the final close-coupling calculation. We used an R-matrix sphere of radius 10 bohrs and continuum Gaussian-type orbitals with partial waves up to $l < 4$. In the following, this calculation will be referred to CAS_1.

Initially, several basis sets—including DZP and cc-pVTZ—were tested to investigate the stability of the target properties such as polarizability and ground state energy and, finally, we chose the cc-pVTZ basis set in order to perform the scattering calculations. Since the first electronically excited state $^3\Sigma_g^-$ is approximately 13 eV above the dissociation limit for the ground state, this latter state is essentially isolated and the non-adiabatic effects are expected to be small. Therefore, for low electron energy collisions, i.e. below 10 eV, only the ground electronic state is open for ionization in e–BF_2^+ collisions, and the dimension of the geometry-fixed scattering matrix remains the same at low collision energies.

At low collision energies the fixed-nuclei scattering matrix depends only weakly on energy. A sharper energy-dependence is observed at certain relatively high energies, corresponding to positions of Rydberg states attached to the excited electronic states of the ion. A quantity convenient for the analysis of the energy dependence of the scattering matrix is the eigenphase sum. Figure 1 displays the eigenphase sum for three different geometries corresponding to a small displacement from equilibrium along each normal mode of the BF_2^+ ion. Bending and asymmetric stretching mode calculations were performed in the C_{2v} abelian subgroup, while for the symmetric mode the group D_{2h} was used in the calculations. The variation of the eigenphase sums is smooth for energies below 6 eV. Above this value, a sharp energy dependence at certain energies is observed due to the presence of electronic Rydberg resonances attached to closed ionization limits.

3. Cross-sections and rate coefficients

For convenience, we introduce the quantities

$$P_i = \frac{g_i}{2} \sum_{ll'\lambda\lambda'} \left| \frac{\partial S_{l\lambda,l'\lambda'}}{\partial q_i} \right|^2, \tag{4}$$

which could be interpreted as the probability of excitation of the vibrational mode *i*, and list them in table 2. Figure 2 shows the weak dependence of those quantities on energy and, therefore, they could be used as constants in calculations of the thermally-averaged rate coefficients.

Using P_i, the cross-sections of equations (1) and (2) are written as

$$\sigma_i^{\rm VE}(E_{\rm el}) = \frac{\pi\hbar^2}{2\,mE_{\rm el}} P_i\,\theta(E_{\rm el} - \hbar\omega_i), \tag{5}$$

$$\sigma^{\rm DR}(E_{\rm el}) = \frac{\pi\hbar^2}{2\,mE_{\rm el}} \sum_{i=1}^{3} P_i\,\theta(\hbar\omega_i - E_{\rm el}). \tag{6}$$

Figure 3 illustrates the DR cross-section $\sigma^{\rm DR}(E_{\rm el})$ computed based on equation (5). At very low scattering energies, i.e. below 0.02 eV, the DR cross-section is a smooth function inversely proportional to the incident energy of the electron, as predicted by the Wigner threshold law, whereas at higher energies, it exhibits a drop at each vibrational threshold.

Due to the simple analytical form of the cross-sections, the corresponding rate coefficients are easily evaluated from the general expression

$$\alpha(T) = \frac{8\pi}{(2\pi k_{\rm b}T)^{3/2}} \int_0^\infty \sigma(E_{\rm el}) \exp\left(-\frac{E_{\rm el}}{k_b T}\right) E_{\rm el}\,{\rm d}E_{\rm el}, \tag{7}$$

giving

$$\alpha_i^{\rm VE}(T) = \sqrt{\frac{2\pi}{k_{\rm b}T}} \frac{\hbar^2}{m^{3/2}} P_i \exp\left(-\frac{\hbar\omega_i}{k_{\rm b}T}\right), \tag{8}$$

$$\alpha^{\rm DR}(T) = \sqrt{\frac{2\pi}{k_{\rm b}T}} \frac{\hbar^2}{m^{3/2}} \sum_{i=1}^{3} P_i \left[1 - \exp\left(-\frac{\hbar\omega_i}{k_{\rm b}T}\right)\right]. \tag{9}$$

where $k_{\rm b}$ is the Boltzmann coefficient and T is the temperature. The thermally-averaged rate coefficients for DR and VE are shown in figure 4.

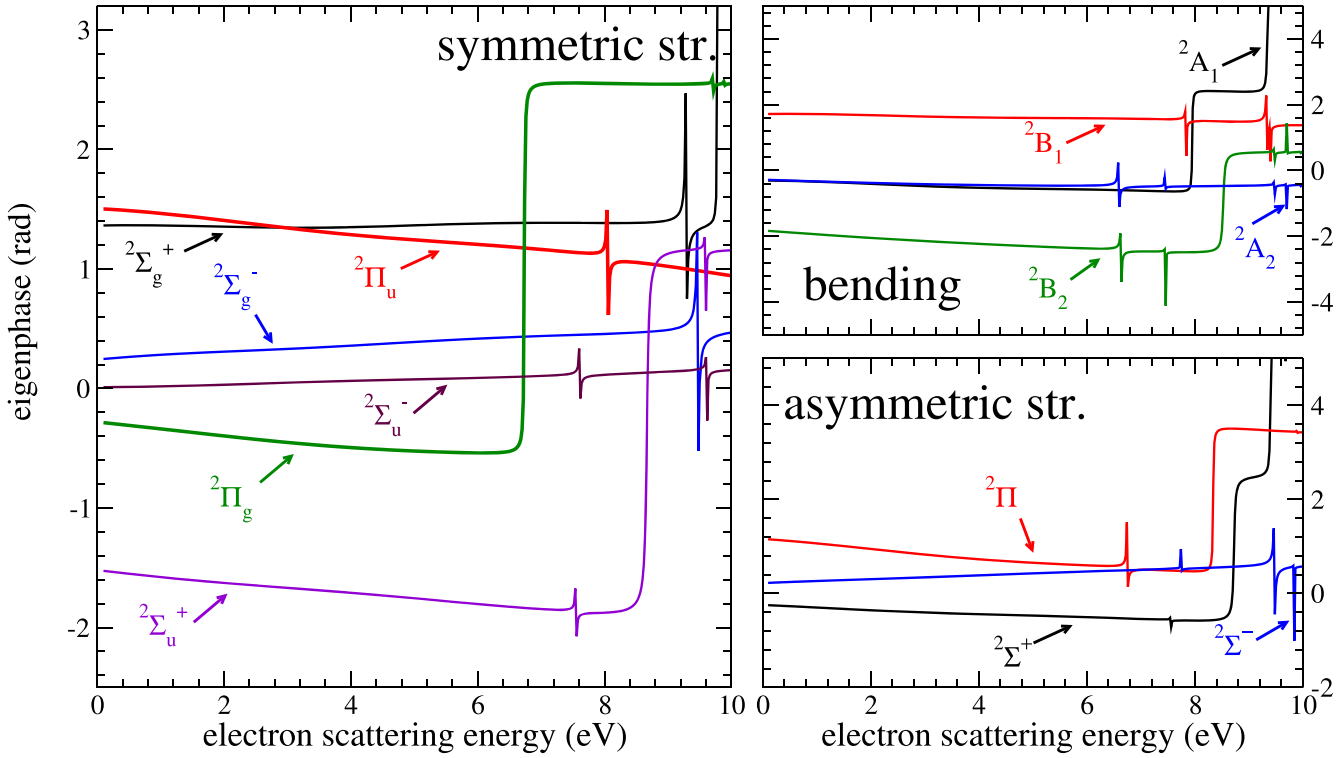

Figure 1. Eigenphase sums as a function of the electron-scattering energy E_{el} for $q_i = 0.01$ (dimensionless) for the symmetric stretching (left panel), bending (right upper panel), and asymmetric stretching (right bottom panel) modes. The curves of different colors correspond to different symmetries of the e^-–BF_2^+ system.

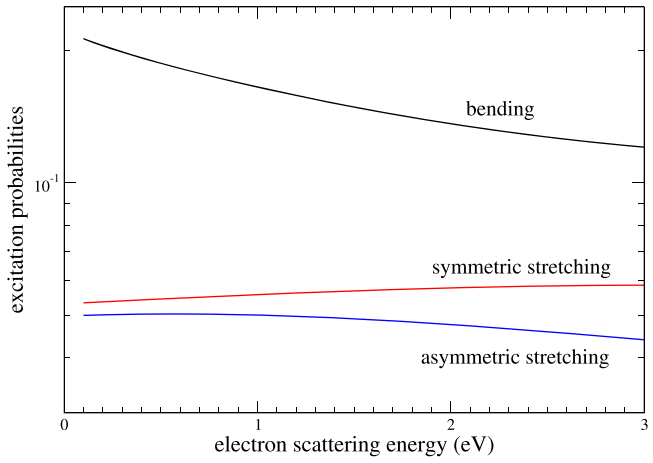

Figure 2. VE of BF_2^+: probabilities corresponding to the normal vibrational modes of the target ion.

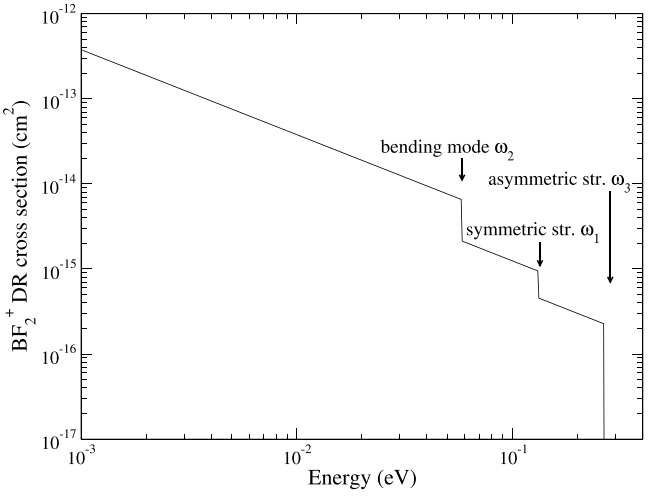

Figure 3. Cross-section for the DR of BF_2^+. The lowest vibrational threshold of each normal mode is indicated by arrows.

Table 2. Parameters of equations (8) and (9) calculated at $E = 0.1$ eV collision energy.

Mode i	P_i
symmetric stretching	0.053
bending	0.20
asymmetric stretching	0.05

In order to access the uncertainty of the present theoretical model, we have performed a complete calculation of the DR and VE rate coefficients using different basis sets and orbital spaces in the electron-scattering calculations. The calculations were performed for three sets of parameters (1) the CAS_1 with the cc-pVTZ basis set, mentioned above; (2) a calculation (referred here as cc-pVTZ CAS_2) similar to (1) but with a smaller orbital space, where 8 electrons are kept free in the active space; and (3) a calculation (referred here as cc-pVQZ CAS_1) similar to (1) but with the larger basis cc-pVQZ. The results are shown in figure 4. The difference between the rate coefficients produced in the three calculations for the DR process and the VE of the asymmetric stretching and bending modes is about 4%. The uncertainty of the rate coefficient for the VE of the symmetric stretching

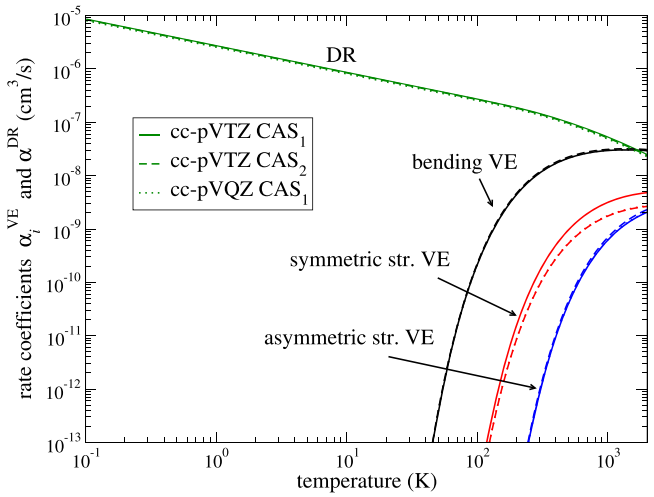

Figure 4. DR and VE of BF_2^+: rate coefficients—equations (8) and (9). To give an idea of the uncertainty of the present results, we also plotted the results of two calculations with the cc-pVTZ CAS_2 (dashed line) and the cc-pVQZ CAS_1 (dotted line) sets of parameters of the model. For the VE of the symmetric stretching mode, the cc-pVTZ CAS_2 and cc-pVQZ CAS_1 curves are indistinguishable and slightly below the cc-pVTZ CAS_1 curve. For the remaining three processes, the three calculations produce curves which are almost indistinguishable in the figure.

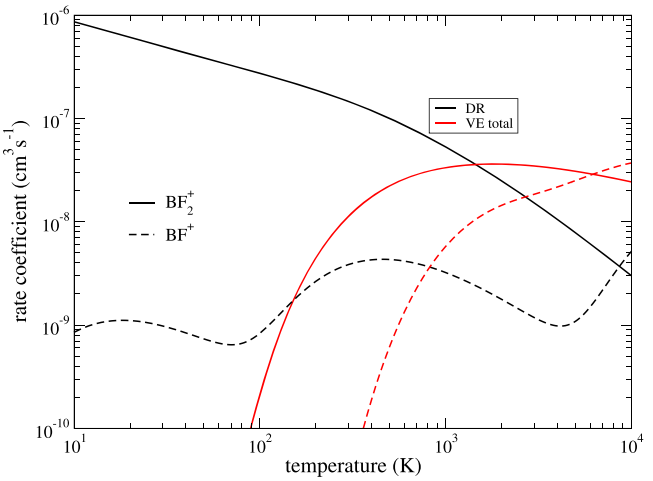

Figure 5. Relative importance of the DR and VE of BF_2^+, with respect to those of BF^+.

mode is larger, varying in the interval 10%–40% for different temperatures. Notice that the overall probability for the symmetric stretching excitation is much smaller than the probabilities for other modes and DR.

4. Conclusions and discussions

In this study, cross-sections and rate coefficients for DR and VE of BF_2^+ by electron-impact were obtained using a theoretical approach that combines the normal modes approximation for the vibrational states of the target ion, the vibrational frame transformation, and the UK R-matrix code. The thermally-averaged rate coefficients have a simple analytical form.

The obtained thermally-averaged rate coefficients are relevant for the kinetic modeling of molecule based cold non-equilibrium plasmas, in the context of a complete lack of other theoretical or experimental data on these processes for this cation, and are ready to be used in the modeling of fluorine/boron plasma for etching or implantation processes. Indeed, we are presently able to make important statements on the relative importance of BF_2^+ with respect to BF^+ on the population and excitation balance. In particular, as shown in figure 5, the DR of BF_2^+ strongly dominates that of BF^+ below 7000 K, and the VE displays the same feature below 5000 K.

The rotational structure of the target ion and of the neutral molecule was neglected in the present approach, which implies that the obtained cross-sections and rate coefficients should be viewed as averaged over initial rotational states and summed over final rotational states of the corresponding initial and final vibrational levels (for VE) or dissociative states (for DR). Purely rotational transitions, i.e. without changing the vibrational state, might be useful to model very cold environments, below 40 K, which is not the case for the presently investigated BF_3 plasma. Moreover BF_2^+ has no permanent dipole, so the rotational transitions are likely to have very small cross-sections.

Acknowledgments

This work was supported by the National Science Foundation, Grant No PHY-1806915.

Ioan F. Schneider and János Zsolt Mezei are grateful for generous financial support from La Région Haute-Normandie, via the GRR Electronique, Energie et Matériaux and the project BIOENGINE, from the Fédération de Recherche 'Energie, Propulsion, Environnement', and from the LabEx EMC^3 and FEDER via the projects PicoLIBS (ANR-10-LABEX-09-01), EMoPlaF and CO_2-VIRIDIS.

They acknowledge support from the CNRS via the GdR THEMS, IAEA (Vienna) via the Coordinated Research Project 'Light Element Atom, Molecule and Radical Behaviour in the Divertor and Edge Plasma Regions', the Programme National 'Physique et Chimie du Milieu Interstellaire' (PCMI) of CNRS/INSU with INC/INP co-funded by CEA and CNES, and Fédération de Recherche 'Fusion par Confinement Magnétique' (CNRS and CEA).

János Zsolt Mezei and Khalid Hassouni acknowledge support from USPC via ENUMPP and Labex SEAM.

Ioan F Schneider thanks Laboratoire Aimé Cotton for its outstanding hospitality.

ORCID iDs

János Zsolt Mezei https://orcid.org/0000-0002-7223-5787

References

[1] Sennikov P G, Kornev R A and Shishkin A I 2017 *Plasma Chem. Plasma Process.* **37** 997
[2] Torigoe M, Teii K and Matsumoto S 2016 *IEEE Trans. Plasma Sci.* **44** 3219
[3] Gonzatti F, Milesi F, Delaye V, Duchaine J, Torregrosa F, Etienne H and Yckache K 2011 *AIP Conf. Proc.* **1321** 27
[4] Duchaine J, Milesi F, Coquand R, Barraud S, Reboh S, Gonzatti F, Mazen F and Torregrosa F 2012 *AIP Conf. Proc.* **1496** 71
[5] Young D L, Nemetti W, La Salvia V, Page M R, Theingi S, Aguiar J, Lee B G and Stardins P 2016 *Sol. Energy Mater. Sol. Cells* **158** 68
[6] Farber M M and Srivastava R D 1984 *J. Chem. Phys.* **81** 241
[7] Yong-Ki K and Irikura K K 2000 *AIP Conf. Proc.* **543** 220
[8] Stewart R A and Lieberman M A 1991 *J. Appl. Phys.* **70** 3481
[9] Lieberman M A and Lichtenberg A J 2005 *Principles of Plasma Discharges and Materials Processing* (Hoboken, New Jersey: John Wiley & Sons, Inc.)
[10] Mezei J Z *et al* 2016 *Plasma Sources Sci. Technol.* **25** 055022
[11] Douguet N, Orel A, Mikhailov I, Schneider I F, Greene C H and Kokoouline V 2011 *J. Phys.: Conf. Series* **300** 012015
[12] Fonseca dos Santos S, Douguet N, Kokoouline V and Orel A E 2014 *J. Chem. Phys.* **140** 164308
[13] Werner H-J *et al* 2012 *WIREs Comput. Mol. Sci.* **2** 242
[14] Pyykko P and Zhao Y 1990 *J. Chem. Phys.* **94** 7753
[15] Perić M and Peyerimhoff S 1993 *Mol. Phys.* **78** 877
[16] Jacox M E and Thompson W E 1995 *J. Chem. Phys.* **102** 4747
[17] Tennyson J 2010 *Phys. Rep.* **491** 29
[18] Carr J, Galiatsatos P, Gorfinkiel J, Harvey A, Lysaght M, Madden D, Mašín Z, Plummer M, Tennyson J and Varambhia H 2012 *Euro. Phys. J.* D **66** 58
[19] Tennyson J, Brown D B, Munro J J, Rozum I, Varambhia H N and Vinci N 2007 *J. Phys. Conf. Series* **86** 012001